Available online at www.sciencedirect.com
SCIENCE DIRECT
ELSEVIER
International Journal of Mass Spectrometry 251 (2006) 179–189
International Journal of Mass Spectrometry
www.elsevier.com/locate/ijms

Stopping highly charged ions in a laser-cooled one component plasma of $^{24}Mg^{+}$ ions

M. Bussmann*, U. Schramm, D. Habs, V.S. Kolhinen, J. Szerypo

Department für Physik Universität München, Am Coulombwall 1, D-85748 Garching, Germany

Received 7 October 2005; received in revised form 22 December 2005; accepted 19 January 2006
Available online 15 March 2006

Abstract

In-trap preparation of highly charged ions (HCIs) for precision mass measurements by cooling in a strongly coupled plasma of laser-cooled $^{24}Mg^{+}$ ions is investigated by molecular dynamics simulations. For HCIs electrostatically decelerated below 1 eV the simulation suggests stopping times of a few 10 μs for high charge states ($Q_{HCI} = 40$, $A_{HCI} = 100$). The deposited energy is found to be distributed almost over the entire crystalline plasma of $N = 10^5$ $^{24}Mg^{+}$ ions due to collective target response. Almost all $^{24}Mg^{+}$ ions stay within the acceptance range of the laser cooling force, thus allowing for the maintenance of the plasma conditions and efficient continuous cooling. Energy loss due to collective effects and hard binary collisions can be clearly distinguished, and can be of the same magnitude for the highest projectile charge states. While the former one can be described by the action of an effective stopping power, the latter is governed by large statistical fluctuations.

PACS: 21.10.Dr; 24.30.Gd; 25.85.Ge; 27.90.+b

Keywords: Simulation; Laser cooling; Penning trap; HCI; Radio frequency quadrupole

1. Introduction

At present buffer gas cooling [1,2], resistive cooling [3], or electron cooling [4] are standard techniques for the cooling of hot ions to the ambient temperature, which in principle can be applied to any ion species of interest. Laser cooling of ions in traps (see [5] and references therein) in comparison is limited to a small number of ion species, while mK temperatures can be reached in shorter cooling times. We discuss a cooling scheme that can reach temperatures almost as low as those reached by laser cooling, while not being restricted to a particular ion species using a cold plasma of laser-cooled ions, into which an ion of another species is injected and cooled. This scheme is known as *sympathetic* cooling.

Cooling of one ion species by another has been studied extensively in traps [6–9]. Here we focus on a method which aims for delivering cold, highly charged ions for precision nuclear mass measurements. A more precise determination of the fine structure constant α for example, or a microscopic definition of the mass unit demand uncertainties of $\Delta m/m \approx 10^{-10}$ in the mass measurement of stable nuclei, while weak interaction studies (the unitarity of CKM matrix or a test of the CVC hypothesis) must be supplied with data on nuclei far from the region of stability measured with a relative precision better than $\Delta m/m \approx 10^{-8}$. In the latter case the typical lifetime of the unstable nuclei determines the maximum duration of the cooling process and the measurement. In combination with low production rates lifetimes below 100 ms demand fast and efficient cooling techniques.

For heavy nuclear masses the most precise measurements have been performed in Penning trap systems [10,11] and besides the now operating systems [12–16] there exists a variety of plans for future systems [17–20].

The measurement accuracy in a Penning trap can be expressed by

$$\frac{\Delta m}{m} \propto \frac{m}{t_{RF} B N_{counts}^{1/2}} \times \frac{1}{Q_{HCI}} \tag{1}$$

where t_{RF} is the measurement time, B the magnetic field, and N_{counts} is the number of measurements with individual ions.

* Corresponding author.
E-mail address: michael.bussmann@physik.uni-muenchen.de (M. Bussmann).

1387-3806/$ – see front matter © 2006 Elsevier B.V. All rights reserved.
doi:10.1016/j.ijms.2006.01.042

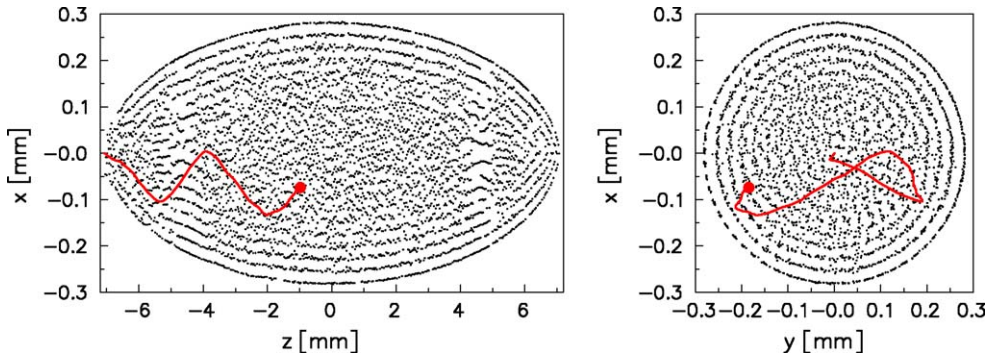

Fig. 1. Trajectory of the HCI through the crystalline plasma in side view (left), the ion having entered from the left, and front view (right). Plasma density: $n_{Mg} = 4.23 \times 10^{13}\,m^{-3}$, initial energy: $E_{kin,HCI} = 300\,meV$, charge state: $Q_{HCI} = 30$, time: $t = 11.4\,\mu s$. Only a slice through the symmetry plane of the crystal is displayed to reveal the crystalline structure.

While increasing the magnetic field is costly and limited in gain, and a significant increase of t_{RF} or N_{counts} might be impossible for radioactive nuclei, breeding ions to higher charge states Q_{HCI} can be readily applied and gives a considerable increase in precision. With highly charged ions relative accuracies of $\Delta m/m \approx 10^{-8} - 10^{-9}$ can be envisaged for $t_{RF} < 100\,ms$. So far the most advanced trap systems in the field, ISOLTRAP at CERN, working with singly charged radioactive ions, and SMILETRAP working with highly charged stable ions, have reached a residual systematic uncertainty of 8×10^{-9} [10] and 10^{-9}–10^{-10} [11], respectively.

In this work we propose a new way of cooling highly charged radioactive ions after charge breeding, typically performed in an electron beam ion source (EBIS), using a combination of electrostatic deceleration of the HCIs and sympathetic cooling in a laser-cooled plasma.

The need for cooling the ions arises from both the ion transport as well as from the accuracy required for precision mass measurements, because the ion bunch suffers from an energy spread of some 10–100 eV, which does not fit the energy acceptance of a precision Penning trap.

Traditional buffer gas cooling in a radio frequency quadrupole (RFQ) cannot be applied to highly charged ions, since charge exchange between the buffer gas atoms and the highly charged ions at a gas pressure of the order of 10^{-1} mbar would result in recombination losses of the high charge states. Resistive cooling requires a cold trap environment and suffers from cooling times longer than the lifetime of short-lived nuclei. Electron or positron cooling is currently investigated (see for example [21]) and also seems promising for in-trap cooling of highly charged ions. The most prominent difference between the ion cooling scheme introduced here and electron cooling schemes is the use of a laser-cooled plasma of ions as a stopping medium instead of electrons cooled by synchrotron radiation. The HCI is injected into the cold one component plasma (OCP) stored in a harmonic potential (see Fig. 1 and the last section for details). The plasma provides a dense, low temperature cooling medium of heavy, charged particles, complementary to standard electron cooling. Demonstrating the feasibility of the stopping of highly charged ions in a laser-cooled OCP of ions requires two demands to be fulfilled:

(1) The HCI should be efficiently stopped in and later extracted from the plasma in a time short enough to allow for fast transport to a precision trap.
(2) The energy deposited in the plasma should not destroy the cold plasma but should instead be distributed over the whole plasma to be quickly cooled by laser cooling.

2. Molecular dynamics simulation of the stopping process

In the following we will use the terms *projectile*, labeling those particles with a high initial energy, usually the HCI, and *target*, labeling the particles of the cooling medium, to distinguish between these two species. Generally the target temperature is kept at an almost constant value via an efficient cooling technique like laser cooling. The cooling rates depend on the strength of the mutual Coulomb-interaction and therefore increase with the square of the charge state of the projectile. Furthermore, the energy transfer is not limited to a finite range of relative projectile–target velocities, and a proper choice of target properties can maximize the heat transfer rate.

Our study focuses on the energy transfer from highly charged ions of some 100 meV initial kinetic energy to a crystalline ensemble of $N = 10^5$ $^{24}Mg^+$ ions confined in a three-dimensional harmonic potential (for a comprehensive list of the parameter region covered please refer to Table 1). The radial confinement Ψ_{radial} is strong compared to the longitudinal confinement Ψ_{long}. In this configuration, normally found in Paul traps or Penning traps the shape of the plasma resembles a prolate ellipsoid of width L_{radial} and length $L_{long} = \alpha L_{radial}$. When the mutual Coulomb-energy of the ions exceeds the kinetic energy at low temperatures, the plasma is strongly coupled, characterized by a plasma parameter $\Gamma = Q_t^2 e^2/(4\pi\epsilon_0 a_{WS} k_B T_t) \geq 1$. For larger values of Γ coupling increases, and the plasma can undergo a phase transition to a crystalline state. In the Coulomb-crystal the ions are ordered in a regular pattern and can interact over a long range. The inter-ion spacing at a plasma density

Table 1
Parameters for the molecular dynamics simulation

Integration time $\Delta\tau_{step}$ (s) 10^{-9}	Lower plasma density	Higher plasma density
Common input parameters		
Ψ_{radial} (V/m^2)	2.5×10^5	3.5×10^5
Ψ_{long} (V/m^2)	2.5×10^3	3.5×10^3
Plasma input parameters		
Number of Mg^+ ions		10^5
A_{Mg}, Q_{Mg}		24, 1
T_{Mg} (K)		10^{-3}
Input parameters for the highly charged ion (HCI)		
Number of highly charged ions		1
A_{HCI}		100
Q_{HCI}		10, 20, 30, 40
$E_{kin,HCI}$ (meV)		100, 200, 300, 400
Plasma properties derived from the simulation		
L_{radial} (m)	632×10^{-6}	565×10^{-6}
L_{long} (m)	15.8×10^{-3}	14.1×10^{-3}
α	25	25
n_{Mg} (m^{-3})	3.02×10^{13}	4.23×10^{13}
$a_{WS}(n_{Mg})$ (m)	19.9×10^{-6}	17.8×10^{-6}
ω_p ($2\pi \times$ MHz)	1.482	1.754
Γ_{Mg}	814	911

n_t is given by the Wigner-Seitz radius $a_{WS} = (4\pi n_t/3)^{-1/3} = (3Q_t e/(8\pi\epsilon_0\Psi_{radial}))^{1/3}$, thus defining a typical length scale of the system. In a strongly coupled plasma the response of the target to the projectile changes significantly compared to the case of a weakly coupled plasma [22], because long-range correlations between the ions are dominant.

In our discussion we frequently use the term *collective* response. It denotes the response of the plasma to the projectile if a major part of all target particles is involved, as, for example, in a plasma wake. In this sense a plasma response due to strong coupling of the target is a collective effect, but collective plasma response does not require strong coupling.

2.1. The simulation model

The creation of the crystalline plasma in a controlled manner is the prerequisite for the simulation. At the start, the $N = 10^5$ ion are placed randomly in the infinite simulation volume and are allowed to propagate freely in the harmonic potential while interacting with each other. Periods of free propagation alternate with periods of strong cooling, until the crystal structure is formed and the individual ion velocities are almost zero. At this point the ion velocities are reset according to the desired temperature, and the plasma is given enough time for equilibration (see Fig. 1 for an impression of the dimensions of the crystalline plasma).

The starting point of the simulation is defined by placing the highly charged ion near the brim of the plasma ellipsoid on the longitudinal symmetry axis of the crystal. The HCI is given an initial kinetic energy with only a velocity component along the longitudinal crystal axis. After a short period the projectile enters the plasma, experiencing subsequent deflections in its binary encounters with the target ions. Fig. 1 shows a typical case of the projectile path through the crystalline plasma, while the vertical and longitudinal dimensions are not to scale to resolve the crystal order.

No laser cooling is included in the simulation, allowing for direct observation of the energy dissipation in the plasma and the development of the velocity distribution of the $^{24}Mg^+$ ions. Laser cooling can be safely omitted as long as the relative velocity v_{rel} can be replaced by the projectile velocity v_p. However if v_p approaches the thermal velocity v_{th} this approximation becomes invalid since the motion of the $^{24}Mg^+$ ions is strongly influenced by the laser.

In the simulation we concentrate on the energy loss due to the Coulomb-interaction of the projectile with the target ions and do not consider other means of energy loss like excitation, ionization and charge exchange [23–25]. Particularly, the ionization time in the two body charge exchange process $^{24}Mg^{1+} + {}^{100}X^{40+} \rightarrow {}^{24}Mg^{2+} + {}^{100}X^{39+}$ can be estimated to several thousand seconds [26]. During the passage of the projectile the Coulomb-interaction of all particles with all particles is computed at each time step, thus including the interaction of target ions with both the projectile and other target ions. This imposes a huge amount of computing power, demanding a parallelization of the simulation.

2.2. Simulation techniques

Systems with a large number of charged particles N are usually treated in simulations using Ewald-summation, multipole expansion or related techniques [27]. These techniques approximate the mutual Coulomb-interaction by computing the Coulomb-force for only a subset of particles, describing the interaction with the remaining particles by a mean field approximation. The approximations are either based on a given symmetry of the system or neglect long-range interactions and are not suitable to simulate a particle traversing through a strongly coupled plasma ellipsoid. It is therefore necessary to explicitly compute the mutual Coulomb-interaction for all N particles in the system.

One can choose to simulate stopping via Coulomb-interaction using either molecular dynamics or Monte Carlo techniques. In the latter case only a small section of the entire stopping volume is regarded, and the total stopping power is calculated by statistically summing up the stopping power due to different particle configurations in this volume. The result gained from this summation generally gives a statistically well-defined mean value for the stopping power. However, this approach fails if the regarded volume and thus the computation time becomes too large, as it is the case here. Long-range interactions of the projectile with the target and correlations of the target ions due to strong coupling suggest to simulate the complete system rather than only a small volume.

Thus a molecular dynamics simulation of the stopping which computes the full $N \times N$ Coulomb-force terms for all particles was chosen in the studied case. Since the computational effort of this task grows by N^2, efficient parallel algorithms [27,28] are used to simulate our model system of $N_{Mg} = 10^5$ $^{24}Mg^+$

particles. Still it remains mandatory to minimize the number of force calculations when integrating the equation of motion

$$m_i \frac{\mathrm{d}^2\vec{r}_i}{\mathrm{d}^2 t} = \left(\sum_{j\neq i}^{N} \frac{q_i q_j}{4\pi\epsilon_0 |\vec{r}_i - \vec{r}_j|^3} (\vec{r}_i - \vec{r}_j) \right) - q_i(\Psi_{\text{radial}}\, x_i, \Psi_{\text{radial}}\, y_i, \Psi_{\text{long}}\, z_i) \quad (2)$$

where m_i, q_i and $\vec{r}_i = (x_i, y_i, z_i)$ are the mass, charge and coordinate vector of the ith particle. This equation of motion is only valid for small relative velocities and is essentially non-relativistic.

To find the optimum balance between accuracy and computation time, we have tested several numerical integrating schemes, including single-step Runge-Kutta and multi-step predictor-corrector methods [27,29]. Most of these integrating schemes are not time reversible and therefore do not preserve energy, which is a vital constraint when simulating sympathetic cooling. The simple, yet effective, Velocity-Verlet [27] algorithm finally chosen requires only two force computations at an accuracy of $(\Delta\tau_{\text{step}})^4$ for an integration time step $\Delta\tau_{\text{step}} = 1$ ns and is energy conserving. The chosen time step satisfies the criterion $\Delta\tau_{\text{step}} \leq \Delta\tau_{\text{stable}} \equiv (16\pi^3\epsilon_0\mu b_{\min}^3/(Q_t Q_p e^2))^{1/2}$ [30] for stable integration of collision kinematics at the minimum impact parameter $b_{\min}$ and for the simulation parameters discussed here we find at minimum $\Delta\tau_{\text{stable}} \approx 4$ ns. Thorough checks of the energy conservation in the system reveal that the simulation is numerically stable for the long simulation period of several thousand time steps, again proving that the integration time chosen is sufficiently small.

An important demand on simulating the mutual interaction of huge numbers of particles is parallelization of the computing algorithm. In this study each time step requires $2N^2 = 2 \times 10^{10}$ computations of the Coulomb-interaction – two for each particle pair, one at time t_0 and one at $t_0 + \Delta\tau_{\text{step}}$. To finish the simulation in a reasonable amount of time while gaining enough information on both the scaling behavior for important parameters as well as systematic errors, it was mandatory to use high end computing power. Fortunately, with the combined computational power of more than three teraflops of two computing clusters housed at our institute and the Leibniz Rechenzentrum, computational time could be lowered to several weeks. To acquire a realistic picture of the stopping dynamics, all particle positions and velocities at each time step were stored on disk for later analysis, and thus several terabyte of data storage were required.

2.3. Modeling the stopping process

Within the linear response model [22] two approaches modeling the target response to the projectile are considered, the binary collision model and the dielectric response model.

In the binary collision model, short-range projectile–target interactions are described by successive binary collisions between the projectile and a target ion. In the dielectric response model, long-range projectile–target interactions are described by the polarization of the plasma induced by the projectile. The impact parameter b can be used to distinguish between these approaches. At small impact parameters the energy loss can be approximated by pure binary collisions, at large impact parameters it can be restricted to collective target response. A simple way of combining both approaches is by writing the energy loss $\mathrm{d}E_p$ per length $\mathrm{d}s$ as the sum of the contributions due to binary collisions and to collective effects as

$$\frac{\mathrm{d}E_p}{\mathrm{d}s} = \int_{b_{\min}}^{b_{\text{trans}}} \frac{\mathrm{d}^2 E_{\text{binary}}}{\mathrm{d}s\mathrm{d}b}\mathrm{d}b + \int_{b_{\text{trans}}}^{b_{\max}} \frac{\mathrm{d}E_{\text{collective}}}{\mathrm{d}s\mathrm{d}b}\mathrm{d}b, \quad (3)$$

choosing appropriate impact parameters $b_{\min}$, $b_{\max}$ and b_{trans}. This choice strongly depends on the properties of projectile and target [22,32], as will be discussed later. The minimum impact parameter is determined by the maximum momentum transfer $b_{\min} = Q_p Q_t e^2/(4\pi\epsilon_0\mu v_{\text{rel}}^2)$. Here Q_p and Q_t are the projectile, and target particle charge numbers and μ is their reduced mass. A common choice for the maximum impact parameter is the adiabatic screening length $b_{\max} = \lambda_{\text{ad}} = v_{\text{rel}}/\omega_p$. Here v_{rel} is the mean relative velocity of projectile and target particles and ω_p is the plasma frequency of the target plasma [22]. In our case this length can be as long as several hundred micrometers and screening lengths of this size can be directly observed in the simulation. For a target plasma of temperature T_t and constituent mass m_t the relative velocity $v_{\text{rel}} = (v_{\text{th}}^2 + v_p^2)^{1/2}$ is defined by the thermal velocity of the target $v_{\text{th}} = (3k_B T_t/m_t)^{1/2}$ and the projectile velocity v_p.

If both the target–projectile and target–target coupling are weak, the energy loss can be written for $v_p \gg v_{\text{th}}$ as [22]

$$\frac{\mathrm{d}E_p}{\mathrm{d}s} = -\frac{Q_p^2 e^2}{4\pi\epsilon_0}\frac{\omega_p^2}{v_p^2}\int_{b_{\min}}^{b_{\max}}\frac{\mathrm{d}b}{b} = \frac{Q_p^2 e^2}{4\pi\epsilon_0}\frac{\omega_p^2}{v_p^2}\Lambda_C(E_p) \propto \frac{\Lambda_C}{E_p}, \quad (4)$$

introducing the Coulomb-logarithm $\Lambda_C \equiv \int_{b_{\min}}^{b_{\max}} \frac{\mathrm{d}b}{b} = \ln(b_{\max}/b_{\min})$ which depends on the kinetic energy of the projectile. The time scale for the response of a target plasma of density n_t to the projectile particle is given by the inverse $\tau_p \equiv \omega_p^{-1}$ of the plasma frequency $\omega_p = (Q_t^2 e^2 n_t/(\epsilon_0 m_t))^{1/2}$. On shorter time scales the target response to the projectile is less pronounced and screening due to target particles is suppressed.

At large projectile velocities compared to the thermal velocity of the target particles the energy loss shows the typical scaling $\mathrm{d}E_p/\mathrm{d}s \propto Q_p^2/E_p$. As the projectile approaches the thermal velocity the energy loss increases drastically, reaching its maximum for $v_p = v_{\text{th}}$. If compared to typical values for electron cooling – $T_{t,e} \approx 10^3$ K, $v_{\text{th,e}} \approx 10^4$ m/s, $n_{t,e} \approx 3 \times 10^{13}$ m^{-3} [33] – the maximum energy loss in a laser-cooled one component plasma of $^{24}Mg^+$ ions ($v_{\text{th,Mg}} \approx 1$ m/s, see Table 1) is roughly $(\mathrm{d}E_{\text{Mg}}/\mathrm{d}s)/(\mathrm{d}E_e/\mathrm{d}s) = m_e v_{\text{th,e}}^2/(m_{\text{Mg}} v_{\text{th,Mg}}^2) \approx 10^3$, assuming similar Coulomb-logarithms and target densities.

In two ways the linear response model is challenged in the studied case. First, it is unable to describe the target response adequately, because it neglects long-range correlations between the constituents of the target. Second, it cannot fully describe the projectile's motion through the plasma, especially at small projectile velocities, since this is affected by the internal target

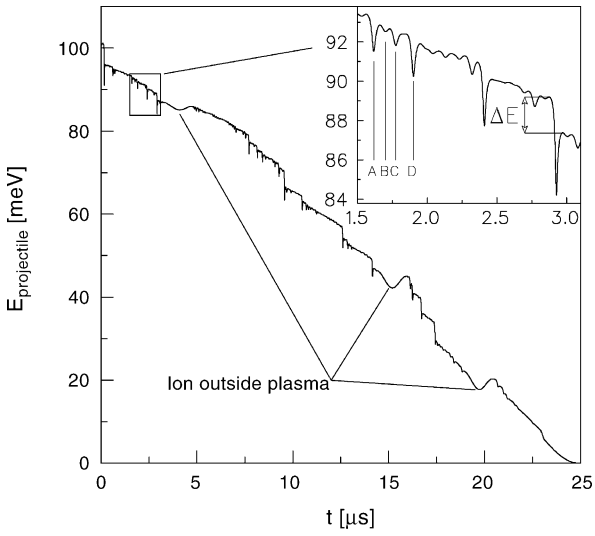

Fig. 2. Kinetic energy of a highly charged ion ($A_{HCI} = 100$, $Q_{HCI} = 10$) during the passage through the $^{24}Mg^{+}$ plasma ($\Gamma_{Mg} = 814$). The insert shows a hard collision with energy loss ΔE in detail and points A, B, C and D indicate successive hard collisions. In addition those times at which the highly charged ion is found outside of the plasma are indicated.

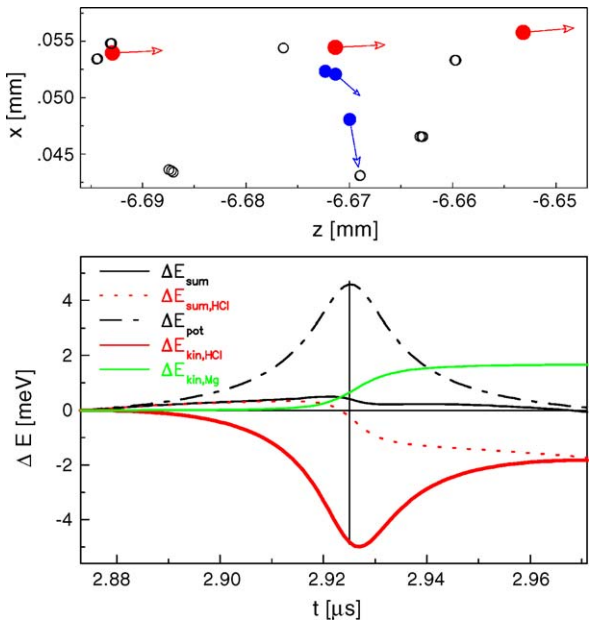

Fig. 3. The upper figure shows three stages of the binary collision denoted by the energy loss ΔE in Fig. 2. The three positions of the ions corresponding to the three stages of the collision are plotted together. Red dots: position of the highly charged ion at (from left to right) the beginning of the collision where the $^{24}Mg^{+}$ ion is still at rest, the moment of closest approach and the end of the collision, blue dots: position of its $^{24}Mg^{+}$ collision partner, black dots: $^{24}Mg^{+}$ ions in their vicinity. The arrows indicate the direction of flight as well as the velocity. The ion positions are shown in projection, thereby losing the depth information. Below: development of the total energy during the collision as described in the text. (For interpretation of the references to color in this figure legend, the reader is referred to the web version of the article.)

configuration. For a correct analysis of the stopping dynamics it is thus vital to use a molecular dynamics simulation which includes these effects.

Fig. 2 shows a typical example of the change in kinetic energy a highly charged ion experiences when passing through the $^{24}Mg^{+}$ crystal. While energy loss due to collective effects leads to a steady decrease in kinetic energy defining the slope of the energy curve, hard binary collisions are characterized by a rapid short-time decrease in the kinetic energy, followed by an equally fast acceleration phase. In the following we will try to analyze both energy loss processes. Due to the low statistics imposed by the huge simulation effort we focus on the energy loss due to collective response, for which we will present results on stopping times.

3. Results

3.1. Energy loss via hard binary collisions

Binary collisions are accurately resolved by the simulation, as seen, for example, at the points labeled A, B, C and D in Fig. 2. The time intervals are well explained by successive collisions of the projectile with velocity $v_{HCI} \approx 420$ m/s with target ions for an average spacing of $a_{WS} \approx 20\,\mu$m. For a single collision the energy loss, denoted ΔE in Fig. 2, will be analyzed in the following. In a pure binary collision the total energy $E_{sum} = E_{kin,HCI} + E_{kin,Mg} + E_{pot}$ is conserved. When the highly charged ion approaches the resting $^{24}Mg^{+}$ the potential energy E_{pot} and the kinetic energy $E_{kin,Mg}$ of the $^{24}Mg^{+}$ increase. The potential energy and the acceleration of the $^{24}Mg^{+}$ reach their maxima at the point of closest approach, indicated by the vertical black line in Fig. 3. The fraction of the potential energy that is not converted into kinetic energy of the $^{24}Mg^{+}$ ion is regained by the passing highly charged ion after the impact.

In Fig. 3 the change in E_{sum} denoted by ΔE_{sum} is plotted from the onset of the collision to its end together with the changes in the kinetic energy of the highly charged ion and the $^{24}Mg^{+}$ ion, $\Delta E_{kin,HCI}$ and $\Delta E_{kin,Mg}$. Additionally the change ΔE_{pot} in potential energy and in the total energy of the highly charged ion, $\Delta E_{sum,HCI} = \Delta E_{kin,HCI} + \Delta E_{pot}$, are depicted.

Unlike in a free binary collision one finds $\Delta E_{sum} > 0$ during the collision. The positive excess can be identified with the binding energy of the $^{24}Mg^{+}$ ion in the crystal lattice. This example shows that the simulation, unlike a simple binary collision approach, is capable of providing insight in the full collision kinematics.

Since the mass of the highly charged ion m_{HCI} is comparable to the $^{24}Mg^{+}$ mass m_{Mg} and fluctuations in the projectile velocity are proportional to $(m_{Mg}/m_{HCI})^{1/2}$ [31], the energy loss in a single, close binary collision can become significantly large compared to the overall energy loss. Thus the summed stopping power of few such encounters can be substantial, although only a small number of $^{24}Mg^{+}$ ions experiences hard collisions with the HCI.

These results show that a correct treatment of the energy loss due to hard binary collisions demands a thorough statistical analysis of the fluctuations in the target velocity. With the data yet available, it is not possible to give a well based

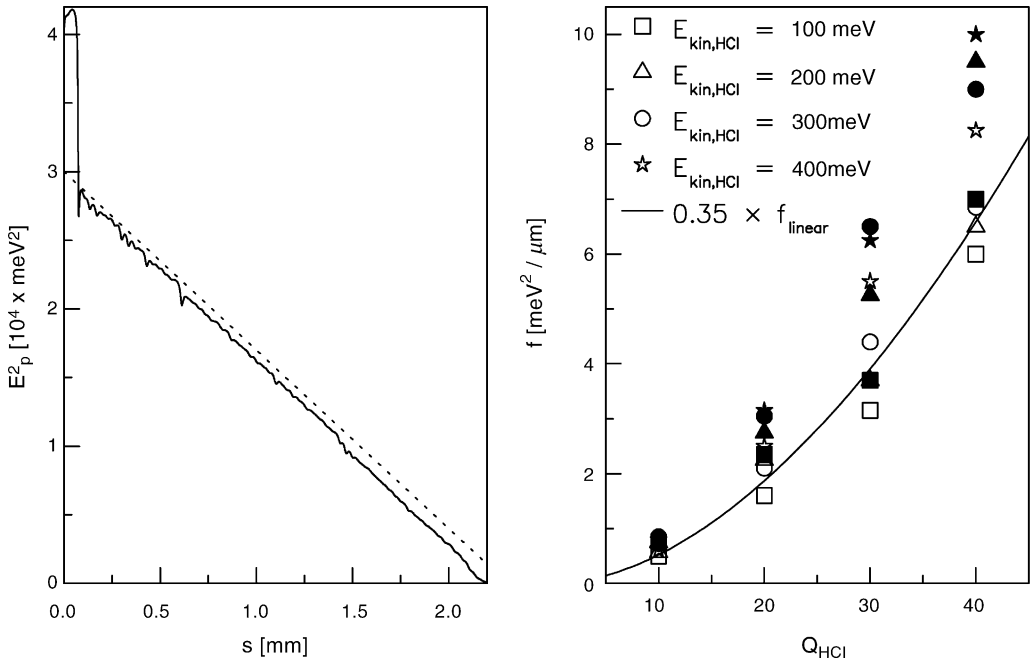

Fig. 4. Left: energy curve ($Q_{\mathrm{HCl}} = 40$, $n_{\mathrm{Mg}} = 3.02 \times 10^{13}\,\mathrm{m}^{-3}$) overlaid with a dashed line of slope $-2f$. Right: the slope f of the energy curve determined by the energy loss in collective scatterings is presented for various initial energies. The solid symbols correspond to $n_{\mathrm{Mg}} = 4.23 \times 10^{13}\,\mathrm{m}^{-3}$, the open symbols to $n_{\mathrm{Mg}} = 3.02 \times 10^{13}\,\mathrm{m}^{-3}$. The solid curve indicates the scaling $f_{\mathrm{linear}} \propto Q^2_{\mathrm{HCl}}$ predicted by linear response theory.

result for $\mathrm{d}^2 E_{\mathrm{binary}}/\mathrm{d}s\mathrm{d}b$. Fortunately, with the computational power available at the Leibniz Rechenzentrum, the statistics will be increased in the future. For increasing charge states the simulations suggest an increase in the contribution of hard binary collisions to the total energy loss, amounting to more than half of the energy loss due to collective response, see Fig. 8.

3.2. Energy loss via collective effects: stopping powers and cooling times

Collective effects can be distinguished from hard binary collisions by setting an upper limit to the kinetic energy carried away by a single $^{24}\mathrm{Mg}^+$ ion, equivalent to a threshold impact parameter b_{trans} above which binary collisions are neglected (see [32] and Eq. (3)). Note, that not only those interactions included in the dielectric response model, but also long-range interactions due to correlations contribute to the energy loss.

Following Eq. (4) one finds $\mathrm{d}E_{\mathrm{p}}/\mathrm{d}s = -f/E_{\mathrm{p}}$, where f is the stopping power multiplied by the projectile energy. This simple approach neglects the weak energy dependence of the Coulomb-logarithm. In the linear response model the factor f can be expressed as

$$f_{\mathrm{linear}} = \frac{Q_{\mathrm{p}}^2 e^2 m_{\mathrm{p}} \omega_{\mathrm{p}}^2}{8\pi\epsilon_0} \times \Lambda_{\mathrm{C}} \xrightarrow[m_{\mathrm{p}} \gg m_{\mathrm{t}}]{v_{\mathrm{p}} \gg v_{\mathrm{rel}}} \frac{Q_{\mathrm{p}}^2 e^2 m_{\mathrm{p}} \omega_{\mathrm{p}}^2}{8\pi\epsilon_0} \times \ln\left(\frac{128^{1/2}\pi\epsilon_0}{Q_{\mathrm{p}} Q_{\mathrm{t}} e^2 m_{\mathrm{p}}^{1/2} \omega_{\mathrm{p}}} E_{\mathrm{p}}^{3/2}\right). \quad (5)$$

Integration yields $E_{\mathrm{p}}^2 = -2fs$. In the left part of Fig. 4 $E^2_{\mathrm{kin,HCI}}$ is plotted versus the path length s denoting the distance the projectile has traveled through the target plasma. If only the overall slope of the energy curve is considered, neglecting the influence of the hard binary collisions, one can deduce an estimate for f as demonstrated by the dotted line. Hard binary collisions lead to steps in the energy curve, but do not alter the continuous slope significantly. This slope is determined by the continuous loss due to simultaneous interactions of the projectile with a large number of target ions, each taking away only a very small fraction of the energy. By fitting a straight line following this general slope, neglecting the large steps caused by hard binary collisions, one can estimate the energy loss due to collective effects. Due to low statistics and systematic errors in fitting a combined error of about 20% is assumed.

These values are plotted in the right part of Fig. 4 versus the projectile charge state. For the special case of $E_{\mathrm{kin,HCI}} = 100\,\mathrm{meV}$ and $n_{\mathrm{Mg}} = 4.23 \times 10^{13}\,\mathrm{m}^{-3}$, corresponding to the solid square data points, the curve $0.35 \times f_{\mathrm{linear}}$ is plotted as a fit to the data points. This suggests that the stopping power due to collective response amounts to about one third of the total stopping power predicted by linear response theory.

The scaling of the data with Q_{HCI} and $E_{\mathrm{kin,HCI}}$ is compared to the scaling predicted by linear response theory. In Fig. 5 all data points are divided by the corresponding value for f_{linear}. Although the statistical basis of single runs in the simulation is weak, a trend can be observed: the scaling of the energy loss with the charge state of the highly charged ion is weaker than expected. We attribute this to enhanced screening as known from the case of electron cooling. No significant change in the energy dependence of the stopping power is found for $v_{\mathrm{p}} \gg v_{\mathrm{th}}$.

If the maximum impact parameter is chosen to be $b_{\max} = \lambda_{\mathrm{ad}}$, one can calculate a value for b_{trans}. Introducing the Coulomb-logarithm $\Lambda_r \equiv \ln(b_{\max}/b_{\mathrm{trans}})$ and the ratio $r \equiv f/f_{\mathrm{linear}}$ one

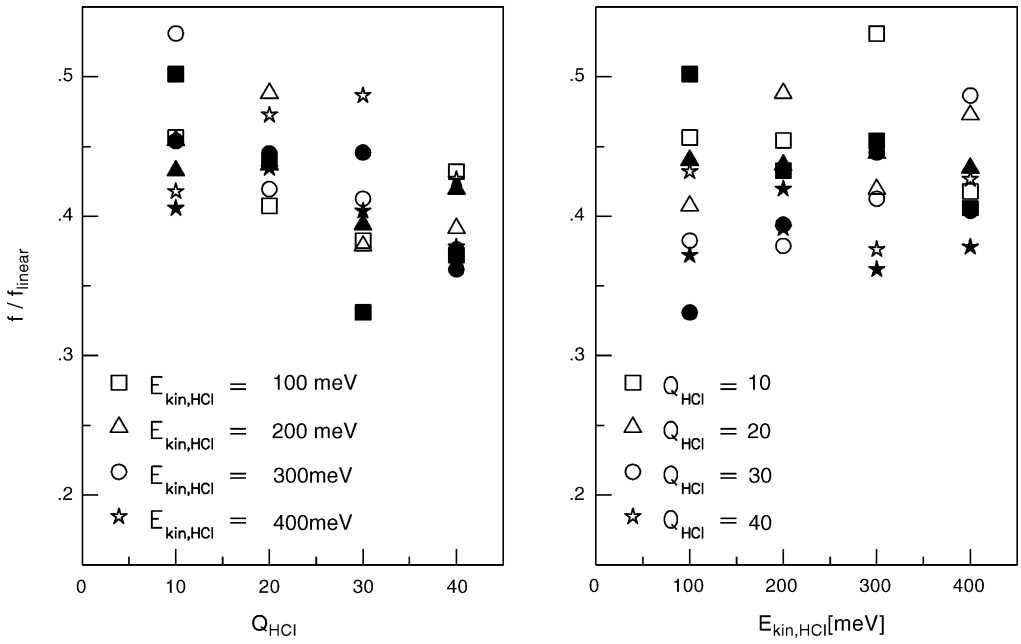

Fig. 5. Scaling of f with charge state (left) and initial kinetic energy (right). The solid symbols correspond to $n_{\mathrm{Mg}} = 4.23 \times 10^{13}\,\mathrm{m}^{-3}$, the open symbols to $n_{\mathrm{Mg}} = 3.02 \times 10^{13}\,\mathrm{m}^{-3}$. The values correspond to the data points found in Fig. 4.

finds $b_{\mathrm{trans}} \equiv (b_{\mathrm{max}}/b_{\mathrm{min}})^{1-r} \times b_{\mathrm{min}}$. With this we approximate f by $(Q_{\mathrm{p}}^2 e^2 m_{\mathrm{p}} \omega_{\mathrm{p}}^2/(8\pi\epsilon_0)) \times \Lambda_r$. For the case of $E_{\mathrm{kin,HCl}} = 100\,\mathrm{meV}$, $n_{\mathrm{Mg}} = 4.23 \times 10^{13}\,\mathrm{m}^{-3}$ and $Q_{\mathrm{HCl}} = 40$ we find $b_{\mathrm{trans}} = 0.64 \times a_{\mathrm{WS}}$ with $r = 0.35$. Following Eq. (3) this would suggest that energy loss due to collective response can be found for impact parameters as low as $0.64 \times a_{\mathrm{WS}}$. The energy transfer in a collision with impact parameter $0.64 \times a_{\mathrm{WS}}$ would amount to $\Delta E = 2Q_{\mathrm{t}}^2 Q_{\mathrm{p}}^2 e^4/((4\pi\epsilon_0)^2 m_{\mathrm{t}} b_{\mathrm{trans}}^2 v_{\mathrm{rel}}^2) \approx 1\,\mathrm{meV}$ [32]. This indicates that linear response theory might be insufficient to give a full description of the stopping dynamics in the studied case.

Plotted in Fig. 6 is the stopping time $\tau_{\mathrm{stop}} = (2m_{\mathrm{p}}E_{\mathrm{p}}^3)^{1/2}/f$ [31], which again only serves as an upper limit to the expected value. Stopping times of a few 10 μs are observed for the high charge states of interest.

A thorough theoretical treatment of the stopping due to collective target response must include further analysis of screening lengths, plasma oscillations and the influence of coupling. This can be achieved by a detailed analysis of the energy deposition in the plasma (see Fig. 7). Though such an analysis goes beyond the scope of this paper, some features of the projectile's passage through the crystal which are related to screening will be

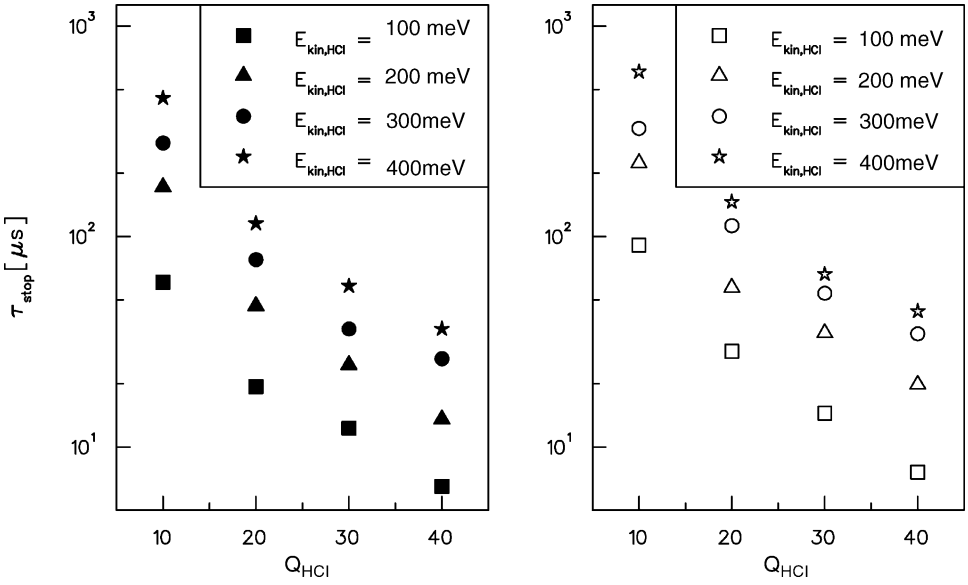

Fig. 6. Stopping times for various initial energies. The solid symbols correspond to $n_{\mathrm{Mg}} = 4.23 \times 10^{13}\,\mathrm{m}^{-3}$, the open symbols to $n_{\mathrm{Mg}} = 3.02 \times 10^{13}\,\mathrm{m}^{-3}$. The values correspond to the data points found in Fig. 4.

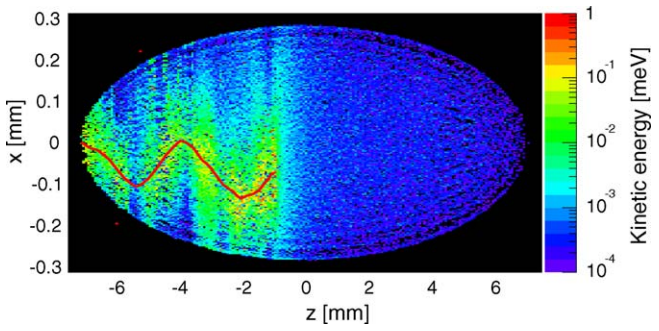

Fig. 7. Spatial distribution of the energy deposited by the HCI after passing through the $^{24}Mg^{+}$ plasma. The color encoded energy values result from a projection of the kinetic energy of the $^{24}Mg^{+}$ ions along the y-axis and are presented in a logarithmic scale. The trajectory of the HCI is shown in red. The corresponding simulation parameters are the same as in Fig. 1. (For interpretation of the references to color in this figure legend, the reader is referred to the web version of the article.)

discussed. From the spatial distribution of the deposited energy one can deduce an upper limit to the interaction radius which has to be taken into account when determining Λ_C. The energy deposition of the projectile in the plasma ranges as far as several hundred micrometers, proving the existence of long-range interactions of the projectile ion with the target ions. The propagation of the deposited energy is determined by the projectile velocity and at early stages of the projectile's passage through the target plasma one finds that the flow of energy in the plasma is slow compared to the projectile velocity. We attribute this to the long time τ_p it takes the plasma to react to the projectile.

3.3. Plasma stability and laser cooling

In all simulated cases the crystalline plasma does not show signs of Coulomb-explosion. Although the energy deposition by the projectile is considerable, the crystalline structure is only locally disturbed. Even in the case of high initial projectile energy and charge state the structural damage remains local, because much of the projectile energy is deposited over the whole plasma volume. The energy loss due to collective effects thus counteracts the local destruction of the crystalline structure due to hard binary collisions and prevents a Coulomb-explosion of the target plasma.

Fast and efficient laser cooling of the target plasma demands that most of the target ions remain within the acceptance of the laser force

$$F_L(\vec{v}_{Mg}) = (\hbar/8) \times |\vec{k}_L| S\Gamma_L^3/((\delta - \vec{v}_{Mg} \cdot \vec{k}_L)^2 + (\Gamma_L/2)^2(1+S)) \quad (6)$$

of typically only few 10 m/s (some 100 μeV). Typically two counterpropagating laser beams with direction $\vec{k}_L$ are applied for cooling, both at negative detuning δ as sketched in Fig. 8. The strength of the resulting laser force is determined by the saturation parameter S. Since a detuning of few Γ_L is needed to maintain a low plasma temperature, the velocity acceptance of the laser force is limited if the laser frequency is not scanned, a procedure that takes considerable time and should thus be avoided. The selection of an appropriate detuning value therefore depends on the velocity distribution of the target plasma after the projectile has deposited its initial energy in the plasma.

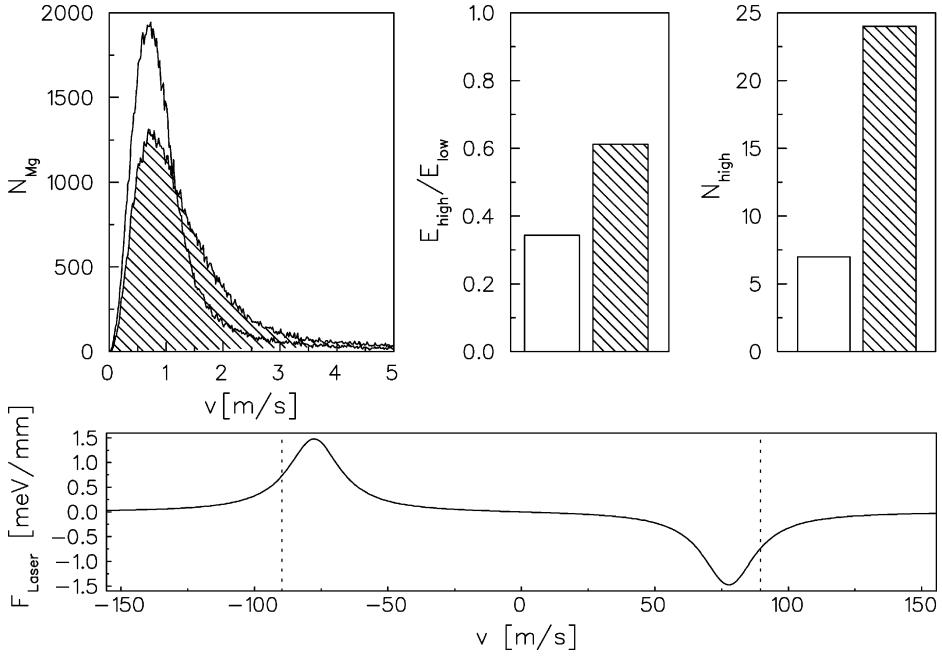

Fig. 8. Upper left: velocity distribution of the $^{24}Mg^{+}$ after the HCI has stopped ($n_{Mg} = 3.02 \times 10^{13}$ m^{-3}). Upper middle: ratio of the total kinetic energy E_{high} of all $^{24}Mg^{+}$ with $E_{kin,Mg} > 1$ meV and the total kinetic energy E_{low} of all $^{24}Mg^{+}$ with $E_{kin,Mg} < 1$ meV. Upper right: number of ions with $E_{kin,Mg} > 1$ meV. The hatched area corresponds to $Q_{HCI} = 40$, $E_{kin,HCI} = 400$ meV, the other to $Q_{HCI} = 10$, $E_{kin,HCI} = 100$ meV. Lower part: combined force of two counterpropagating laser beams as given in Eq. (6) ($\delta = 6.5 \times \Gamma_L$, $S = 3$, transition wavelength $\lambda_L = 2\pi/|\vec{k}_L| = 280$ nm, natural linewidth $\Gamma_L = 2\pi \times 42.7$ MHz). The dashed lines at $v = \pm 90$ m/s correspond to an ion energy of $E_{kin,Mg} = 1$ meV.

The upper left part of Fig. 8 shows two examples of the final velocity distribution of the plasma ions. For a detuning of $\delta = 6.5 \times \Gamma_L$ all $^{24}Mg^+$ ions with $E_{kin,Mg} < 1$ meV or $v_{Mg} = 90$ m/s are in the acceptance of the laser force. In the middle part the total kinetic energy of all $^{24}Mg^+$ ions with $E_{kin,Mg} > 1$ meV is set in relation to the total kinetic energy of those $^{24}Mg^+$ ions with $E_{kin,Mg} < 1$ meV. The total number of the ions with $E_{kin,Mg} > 1$ meV is negligibly small as can be seen in the upper right part of the figure. Nevertheless the amount of the total kinetic energy carried away by these hot ions is considerable. Further studies must show whether these ions are sympathetically cooled by the cold ions or if a sort of evaporative cooling can be applied.

4. Experimental realization of the cooling scheme

Inside an Electron Beam Ion Source (EBIS) atoms of interest for precision mass measurements undergo an ionization cascade in collisions with energetic electrons until the desired charge state is reached after few 10 ms. The resulting ion beam consists of an ensemble of ions of varying charge state and energy and can be characterized by an extraction time τ_{EBIS} after which 90% of the ions are extracted. To adjust the kinetic energy of the HCIs exiting the EBIS with an energy spread of some 10–100 eV to the level where ion cooling as described above is most efficient, we propose the use of a segmented linear radio frequency quadrupole (RFQ) system. In such a linear Paul trap ions are radially confined by a radio frequency quadrupole field of frequency Ω_{RF} if $0 < q \ll 0.9$. The stability parameter $q \approx \frac{1}{\Omega}\sqrt{8\frac{Qe}{m}\Psi_{radial}}$ depends on the particle's charge to mass ratio Qe/m. By adjusting the strength and frequency of the radial confinement field, ions of different species and charge state can be trapped and cooled together [5].

A pulsed beam of HCIs coming from the EBIS is transferred into the RFQ. The pulse duration, the energy spread ΔE_{EBIS} and the desired efficiency determine the length L_{RFQ} of the RFQ.

Assuming a rectangular pulse shape one can introduce an injection efficiency p_{inj} determining the fraction of ions that are trapped in the RFQ and its length is then given by $L_{RFQ} = \tau_{EBIS}\, p_{inj}\, (Q_{HCI}\, e\, \Delta E_{EBIS}/(2m_{HCI}))^{1/2}$. For the proposed cooling scheme shortening the RFQ results in shorter cooling times for the sacrifice of a decrease in injection efficiency. This decrease can be compensated if shorter pulses are achieved – for example by using fast extraction schemes [34]. Optimizing the overall duration and efficiency of both charge breeding and cooling for a specific ion of interest requires careful tuning of the EBIS ion beam parameters to the acceptance of the RFQ cooler.

During the cooling the ions in the RFQ are trapped in a potential well $U_{RFQ}(z)$ along the beam direction z by applying different voltages to the electrode segments (see Fig. 9). Opposite to the injection region of the RFQ the $^{24}Mg^+$ ions are laser-cooled in a potential well separated from the trapping region, while the HCI oscillate in the trapping region. When the trapping potential is raised those highly charged ions with sufficient energy to overcome the barrier separating the trapping region from the cooling region enter the laser-cooled $^{24}Mg^+$ plasma, which can be detected by a change in the fluorescence of the $^{24}Mg^+$ ions. By constantly rising the trapping potential, all highly charged ions can be successively cooled, stored and detected in the cooling region. For efficient cooling the difference in kinetic energy between the HCI and $^{24}Mg^+$ ions should be kept as small as possible (see Eq. (4)).

The overall storage period for all HCIs trapped depends on the length L_{RFQ} of the RFQ and the energy spread of the HCI beam. While the length of the RFQ determines the maximum time it requires for a highly charged ion to reach the cooling region, the energy spread determines the overall raise of the trapping potential with respect to the cooling region. The system can be optimized for either high efficiency or fast cooling, depending on the ion of interest. For rare short-lived ions, detected in the cooling region, the cycle could even be stopped for immediate transfer to the measurement trap. In this operation mode the time for the electrostatic deceleration can be kept small compared to the time needed for cooling and ejection of the HCI.

Those highly charged ions stopped in the plasma of laser-cooled $^{24}Mg^+$ reside in the cooling region and must be extracted to be transferred to the precision Penning trap. One method of extraction is to lower the potential at the RFQ exit leading to the precision Penning trap while holding back the $^{24}Mg^+$ ions by

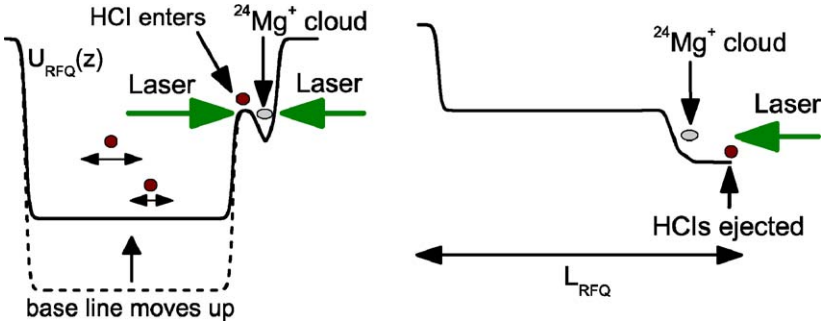

Fig. 9. Left: sketch of the longitudinal potential gradient during the cooling. The trap is divided in a long trapping section and a small cooling section where the $^{24}Mg^+$ ions are located. During the cooling the base line of the storing section potential is continuously raised. Right: potential configuration for the extraction of the HCIs. The laser force keeps the $^{24}Mg^+$ ions inside the trap while the HCIs are ejected.

the laser force. If the HCIs are positioned close to the edge of the plasma they travel along the potential gradient towards the RFQ exit while the counteracting laser force prevents the loss of the $^{24}Mg^{+}$ ions. The advantages of this extraction scheme are two-fold. First, no reloading of $^{24}Mg^{+}$ ions is necessary after the extraction of the cooled highly charged ions. Second, reheating of the cool ensemble of highly charged ions during extraction can be minimized by adjusting the potential gradient. Since the laser has to counteract the potential gradient to avoid a loss of plasma ions the potential gradient E_{extract} cannot be greater than some meV per mm. Fortunately the corresponding acceleration force $F_{\text{extract}} = Q_{\text{HCI}}\, e\, E_{\text{extract}}$ grows with the charge state. Still, extraction times of the ions might be constrained by shielding effects in the cold plasma and the small potential gradient. In the future we plan to simulate this extraction scheme.

5. Conclusion and outlook

We have shown that efficient stopping of low energy highly charged ions in a one component plasma of laser-cooled $^{24}Mg^{+}$ is possible, providing cooling times of a few 10 μs once the ion is prepared at sub-eV energies. Many important properties of the stopping process can be modeled using classical linear response theory. Nevertheless, the determination of absolute values for the stopping power requires a well-justified definition of the correct range of projectile–target interactions. This definition demands a separate treatment of energy loss due to hard collisions and collective effects. While the latter can be described by an effective energy loss the former can only be treated defining an average stopping power deduced from statistically summing the results of consecutive measurements. Fully understanding the complexities of the stopping process remains an open task which we plan to address in the future. This includes studies of the collective response of the crystalline plasma and a comparison with electron and positron cooling. Furthermore, recent results not included here suggest only a weak dependence of the stopping power on the strength of the target coupling, promising similar stopping power for moderately laser-cooled plasmas. To conclude, we believe that ion cooling can become an important tool in future precision mass experiments.

Acknowledgments

The authors want to thank Jürgen Kluge for many inspiring interactions, keeping atomic and laser physics stirring at GSI. M. Bussmann would furthermore like to thank M. Schubert (LS Habs) and R. Bader (LRZ) for their invaluable help with the computer clusters which were used in the simulation. This work was partially supported by Leibniz Rechenzentrum project UH351AE.

References

[1] G. Savard, St. Becker, G. Bollen, H.-J. Kluge, R.B. Moore, Th. Otto, L. Schweikhard, H. Stolzenberg, U. Wiess, Phys. Lett. A 158 (1991) 247.
[2] F. Herfurth, J. Dilling, A. Kellerbauer, G. Bollen, S. Henry, H.-J. Kluge, E. Lamour, D. Lunney, R.B. Moore, C. Scheidenberger, S. Schwarz, G. Sikler, J. Szerypo, Nucl. Instrum. Methods Phys. Res., Sect. A 469 (2001) 254.
[3] H. Häffner, T. Beier, S. Djekić, N. Hermanspahn, H.-J. Kluge, W. Quint, S. Stahl, J. Verdú, T. Valenzuela, G. Werth, Eur. Phys. J. D 22 (2003) 163.
[4] G. Gabrielse, X. Fei, L.A. Orozco, R.L. Tjoelker, J. Haas, H. Kalinowsky, T.A. Trainor, W. Kells, Phys. Rev. Lett. 63 (1989) 1360.
[5] U. Schramm, D. Habs, Prog. Part. Nucl. Phys. 53 (2004) 583.
[6] D.J. Larson, J.C. Bergquist, J.J. Bollinger, W.M. Itano, D.J. Wineland, Phys. Rev. Lett. 57 (1986) 70.
[7] P. Bowe, L. Hornekær, C. Brodersen, M. Drewsen, J.S. Hangst, Phys. Rev. Lett. 82 (1999) 2071.
[8] B. Roth, U. Fröhlich, S. Schiller, Phys. Rev. Lett. 94 (2005) 053001-1.
[9] S. Toleikis, R. Maruyama, D.A. Church, D. Schneider, S.J. Freedman, I. Kominis, P.A. Vetter, Nucl. Instrum. Methods Phys. Res., Sect. B 235 (2005) 479.
[10] A. Kellerbauer, K. Blaum, G. Bollen, F. Herfurth, H.-J. Kluge, M. Kuckein, E. Sauvan, C. Scheidenberger, L. Schweikhard, Eur. Phys. J. D 22 (2003) 53.
[11] T. Fritioff, H. Bluhme, R. Schuch, I. Bergström, M. Björkhage, Nucl. Phys. A 723 (2003) 3.
[12] I. Bergström, C. Carlberg, T. Fritioff, G. Douysset, J. Schönfelder, R. Schuch, Nucl. Instrum. Methods Phys. Res., Sect. A 487 (2002) 618.
[13] G. Bollen, F. Ames, G. Audi, D. Beck, J. Dilling, O. Engels, S. Henry, F. Herfurth, A. Kellerbauer, H.-J. Kluge, A. Kohl, E. Lamour, D. Lunney, R.B. Moore, M. Oinonen, C. Scheidenberger, S. Schwarz, G. Sikler, J. Szerypo, C. Weber, The ISOLDE Collaboration, Hyperfine Interact. 132 (2001) 215.
[14] G. Savard, R.C. Barber, C. Boudreau, F. Buchinger, J. Caggiano, J. Clark, J.E. Crawford, H. Fukutani, S. Gulick, J.C. Hardy, A. Heinz, J.K.P. Lee, R.B. Moore, K.S. Sharma, J. Schwartz, D. Seweryniaki, G.D. Sprouse, J. Vaz, Hyperfine Interact. 132 (2001) 223.
[15] V.S. Kolhinen, S. Kopecky, T. Eronen, U. Hager, J. Hakala, J. Huikari, A. Jokinen, A. Nieminen, S. Rinta-Antila, J. Szerypo, J. Äystö, Nucl. Instrum. Methods Phys. Res., Sect. A 528 (2004) 776.
[16] G. Marx, J. Dilling, H.-J. Kluge, M. Mukherjee, W. Quint, S. Rahaman, D. Rodriguez, G. Sikler, M. Tarisien, C. Weber, SHIPTRAP Collaboration, Hyperfine Interact. 146/147 (2003) 245.
[17] J. Dilling, P. Bricault, M. Smith, H.-J. Kluge, The TITAN Collaboration, Nucl. Instrum. Methods Phys. Res., Sect. B 204 (2003) 492.
[18] S. Schwarz, G. Bollen, D. Lawton, P. Lofy, D.J. Morrissey, J. Ottarson, R. Ringle, P. Schury, T. Sun, V. Varentsov, L. Weissman, Nucl. Instrum. Methods Phys. Res., Sect. B 204 (2003) 507.
[19] W. Quint, J. Dilling, S. Djekić, H. Häffner, N. Hermanspahn, H.-J. Kluge, G. Marx, R. Moore, D. Rodriguez, J. Schönfelder, G. Sikler, T. Valenzuela, J. Verdú, C. Weber, G. Werth, Hyperfine Interact. 132 (2001) 457.
[20] J. Szerypo, D. Habs, S. Heinz, J. Neumayr, P. Thirolf, A. Wilfart, F. Voit, Nucl. Instrum. Methods Phys. Res., Sect. B 204 (2003) 512.
[21] K. Blaum, MATS Collaboration, MATS technical proposal (FAIR/NUSTAR LOI Identification No. 8, 2005).
[22] G. Zwicknagel, C. Toepffer, P.-G. Reinhard, Phys. Rep. 309 (1999) 117.
[23] With ionisation energies of $\Delta E(^{24}Mg^{1+} \rightarrow {}^{24}Mg^{2+}) = 1.527\,\text{eV}$ and $\Delta E(^{24}Mg^{2+} \rightarrow {}^{24}Mg^{3+}) = 7.871\,\text{eV}$ respectively ionisation and excitation can be safely neglected. See T.A. Carlson, C.W. Nestor Jr., N. Wasserman, J.D. McDowell, At. Data Nucl. Data Tables 2 (1970) 63.
[24] H. Cederquist, C. Biedermann, N. Selberg, P. Hvelplund, Phys. Rev. A: At., Mol., Opt. Phys. 51 (1995) 2191.
[25] B.R. Beck, J. Steiger, G. Weinberg, D.A. Church, J. McDonald, D. Schneider, Phys. Rev. Lett. 77 (1996) 1735.
[26] R.E. Olson, A. Salop, Phys. Rev. A: At., Mol., Opt. Phys. 14 (1976) 579.
[27] G. Sutmann, In: J. Grotendorst, D. Marx, M. Muramatsu(Ed.), Quantum Simulations of Complex Many-Body Systems, NIC Series, vol. 10, John von Neumann Institue for Computing, Jülich, 2002, p. 211.
[28] S. Plimpton, B. Hendrickson, J. Comput. Chem. 17 (1996) 326.

[29] G. Engeln-Müllges, F. Uhlig, Numerical Algorithms with C Springer, Berlin, Heidelberg and New York, 1996.
[30] R.W. Hockney, J.W. Eastwood, Computer Simulation using Particles, Adam Hilger, Bristol and Philadelphia, 1988.
[31] A.H. Sørensen, E. Bonderup, Nucl. Instrum. Methods Phys. Res. 215 (1983) 27.
[32] H. Poth, Phys. Rep. 196 (1990) 135.
[33] A. Wolf, Wechselwirkung zwischen hochgeladenen Ionen und freien Elektronen in einem Ionenspeicherring. MPI-K Heidelberg Report, vol. 15, 1992.
[34] O. Kester, Entwicklung einer Elektronenstrahlionenquelle mit "schneller" Ionenextraktion zur Anwendung bei der Strahlentherapie mit leichten Ionen (Dissertation Johann-Wolfgang-Goethe Universität, Frankfurt, 1995).